# POST LAUNCH STUDY

# REPORT OF VAS-D PERFORMANCE

A Report Under NASA Contract NAS5-21965

by

Paul Menzel

March 1981

The University of Wisconsin
Space Science and Engineering Center
1225 West Dayton Street
Madison, WIsconsin 53706

TABLE OF CONTENTS

## INTRODUCTION

The GOES-D spacecraft was launched September 9, 1980 with the first VISSR Atmospheric Sounder (VAS) on board. After two weeks of station keeping maneuvers, the VAS-D began transmitting engineering checkout and sounding radiance data. This report is an update of the Prelaunch Study Report of VAS-D Performance and is based on analyses of inflight data.

One month before launch it was confirmed that the upper large HgCdTe detector on VAS-D had failed. The effect of this failure on the dwell sounding and multispectral imaging modes of operation is discussed.

The electronic calibration of the detectors was investigated and the linearity of the detector response was catalogued. VAS-D radiometric determinations were compared with determinations from the NOAA-6 HIRS radiometer and with radiosonde measurements to assess the validity of the VAS calibration.

An error was found in the prelaunch evaluation of single sample noise. Corrected values are presented. The reduction of noise by multiple scanning was analyzed and the results were compared with prelaunch estimates. A new spin budget is determined.

Initial determinations of the misregistration of images from different detectors were made. Our findings are summarized.

# I. INFLIGHT VAS-D CALIBRATION

Two types of inflight calibration were performed on the VAS instrument: electronic, by a precision waveform for the infrared channels; and radiometric, by an internal blackbody for all infrared spectral bands.

## Electronic Calibration

A precision voltage waveform is inserted at the preamplifier input of all channels. The ramp waveform as seen at the channel output is shown in Figure I. 1. The ramp waveform is synchronized to the satellite supplied Decom Sync signal.

On a scan line containing the calibration waveform, the channel offset level will be present for 100 μsec following the Decom Sync timing signal; the channel offset is then removed from the channel output for 3.5 msec (0.0 volt level) and then the ramp waveform starts (3.6 msec from the Decom Sync timing signal). The ramp slope is 0.312 volt/msec for 16.20 msec. This will give a nominal upper dc value of 5.06 volts, ensuring complete dynamic range calibration. After the completion of the ramp, the electronic calibration waveform will fall back to a 4.50 volt level for 1.8 msec. This level can be used for a single point gain level check. The waveform will then return to 0.0 volt for 3.6 msec when the channel offset level will be replaced.

The electronic calibration sequence is programmable ON/OFF via the VAS on-board processor using parameter P35. When the electronic calibration is programmed ON by parameter selection and the electronic calibration has been enabled by satellite command, the electronic calibration waveform will appear for eight successive spins beginning with the fourth satellite spin following the receipt of a Step Scan ON command. The two infrared channels will output the waveforms that have passed through the amplifier/gain circuits associated with the following

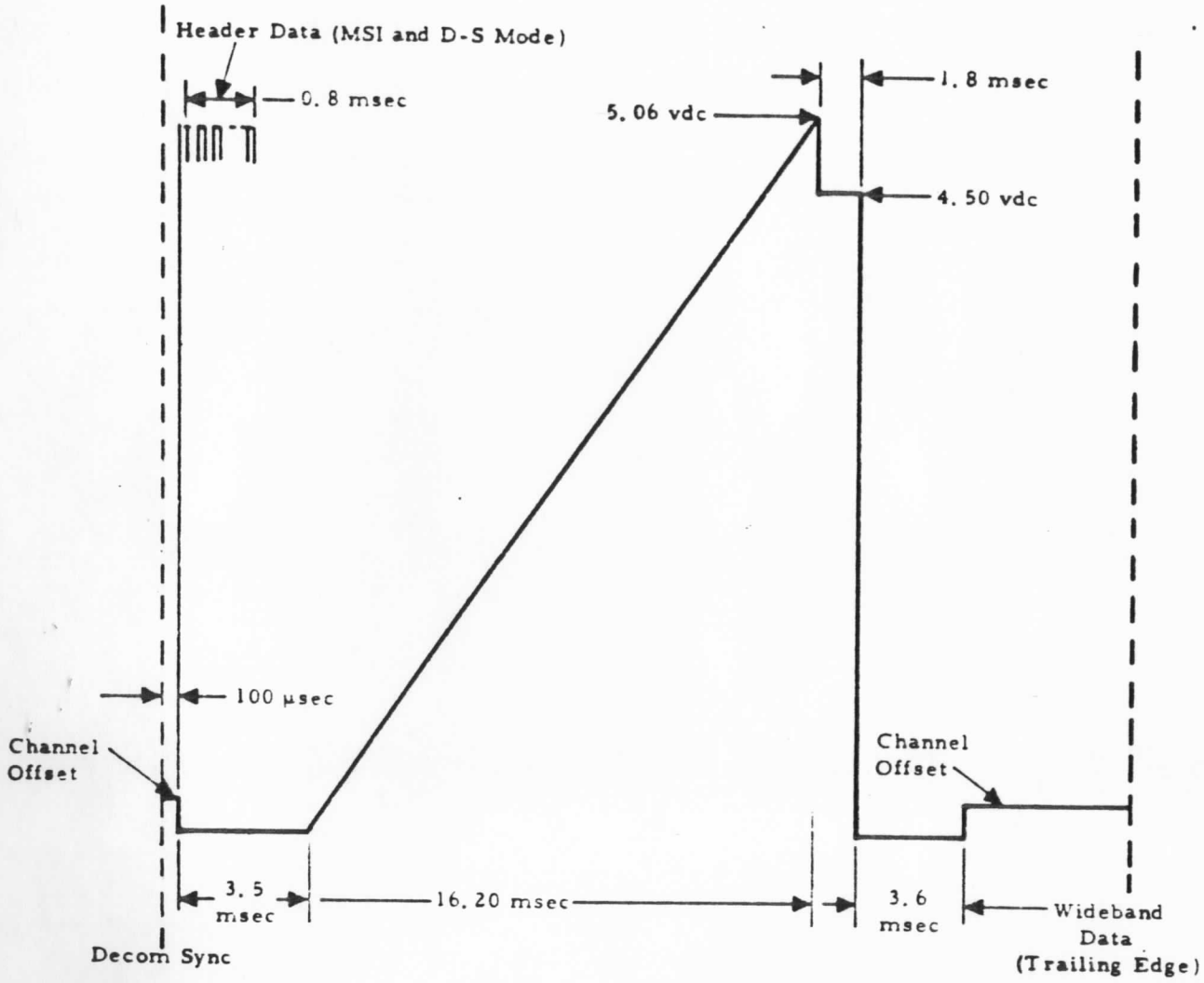


Figure I.1 Calibration Ramp Waveform as seen at the Channel Output.

spectral bands and detector sizes, for the spin number shown:

Spin No. 4, Spectral Band No. 8 - Large Detector
Spin No. 5, Spectral Band No. 8 - Small Detector
Spin No. 6, Spectral Band No. 12 - Large Detector
Spin No. 7, Spectral Band No. 9 - Large Detector
Spin No. 8, Spectral Band No. 9 - Small Detector
Spin No. 9, Spectral Band No. 4 - Large Detector
Spin No. 10, Spectral Band No. 4 - Small Detector
Spin No. 11, Spectral Band No. 11 - Large Detector

On the twelfth spin, a 3.00-vdc check voltage will be placed on the infrared channel (spectral band No. 8 - small detector) sample-and-hold circuit and held until the thirteenth spin as a calibration check of the sample-and-hold circuit.

Tables I. 1 and I. 2 summarize the inflight measurements of the calibration waveform. The average ramp slope was found to be .308 volt/msec (within 1% of the specified value) and the average plateau voltage was determined to be 4.42 volts (within 2% of the specified value). The data confirms that the upper large HgCdTe detector has failed. The observed noise level for band 8 is noticeably lower than the other bands, while for band 9 it is noticeably higher.

Radiometric Calibration

As described in the Prelaunch Study Report of VAS-D Performance, the coefficients for the calibration algorithm were determined from thermal vacuum tests. This algorithm relates the internal calibration blackbody radiance to an equivalent external blackbody radiance which gives rise to the same channel output voltage. This is accomplished by modelling the contribution of the VAS telescope foreoptics components to background radiation. The relationship has the form

$$N_B = R_{bb} + \sum_i c_i \, (R_{bb} - R(T_i))$$

Table I.1 VAS-D Electronic Calibration Ramp

| filter | detector | ramp slope (volts/msec) | offset (volts) | linear regression coefficient | σ ramp (volts) |
|---|---|---|---|---|---|
| 8 | Upper Large HgCdTe | | no calibration ramp | | |
| 8 | Lower Large HgCdTe | .309 | -.717 | .9999 | .004 |
| 8 | Upper Small HgCdTe | .312 | -.760 | .9999 | .007 |
| 8 | Lower Small HgCdTe | .306 | -.717 | .9999 | .007 |
| 12 | Upper Large InSb | .309 | -.642 | .9990 | .051 |
| 12 | Lower Larger InSb | .304 | -.596 | .9982 | .067 |
| 9 | Upper Large HgCdTe | | no calibration ramp | | |
| 9 | Lower Large HgCdTe | .305 | -.738 | .9974 | .080 |
| 9 | Upper Small HgCdTe | .306 | -.712 | .9875 | .177 |
| 9 | Lower Small HgCdTe | .307 | -.756 | .9885 | .170 |
| 4 | Upper Large HgCdTe | | no calibration ramp | | |
| 4 | Lower Large HgCdTe | .310 | -.728 | .9998 | .024 |
| 4 | Upper Small HgCdTe | .311 | -.779 | .9985 | .062 |
| 4 | Lower Small HgCdTe | .310 | -.732 | .9987 | .057 |
| 11 | Upper Large InSb | .310 | -.652 | .9989 | .052 |
| 11 | Lower Large InSb | .307 | -.602 | .9980 | .071 |

Table I.2 VAS-D Electronic Calibration Plateaus

| filter | detector | zero (volts) | | offset (volts) | | plateau (volts) | |
|---|---|---|---|---|---|---|---|
| | | $\bar{z}$ | $\sigma_z$ | $\bar{o}$ | $\sigma_o$ | $\bar{p}$ | $\sigma_p$ |
| 8 | ULH | | | no waveform | | | |
| 8 | LLH | .015 | .004 | .265 | .005 | 4.435 | .006 |
| 8 | USH | .001 | .016 | .257 | .005 | 4.461 | .013 |
| 8 | LSH | .006 | .006 | .260 | .006 | 4.391 | .007 |
| 12 | ULI | .012 | .018 | .261 | .014 | 4.448 | .018 |
| 12 | LLI | .023 | .029 | .267 | .017 | 4.405 | .016 |
| 9 | ULH | | | no waveform | | | |
| 9 | LLH | .031 | .038 | .150 | .099 | 4.342 | .076 |
| 9 | USH | .121 | .152 | .287 | .173 | 4.413 | .202 |
| 9 | LSH | .026 | .051 | .219 | .217 | 4.321 | .169 |
| 4 | ULH | | | no waveform | | | |
| 4 | LLH | .036 | .023 | .287 | .023 | 4.463 | .027 |
| 4 | USH | .017 | .034 | .239 | .047 | 4.413 | .067 |
| 4 | LSH | .014 | .021 | .244 | .063 | 4.416 | .063 |
| 11 | ULI | .011 | .018 | .268 | .019 | 4.459 | .022 |
| 11 | LLI | .020 | .017 | .266 | .017 | 4.443 | .019 |

where

$N_B$ = equivalent external blackbody radiance

$R_{bb}$ = internal blackbody radiance

$C_i$ = calibration coefficients

and $R(T_i)$ = radiance emanating from $i^{th}$ component and temperature $T_i$.

To evaluate the inflight reliability of this calibration procedure, the VAS radiance determinations were compared to NOAA-6 High resolution Infrared Radiation Sounder (HIRS) radiance determinations. This was accomplished as follows.

From a statistical sample of radiosonde-rocketsonde data (the NESS 1200 sample sounding set) and transmittance functions for the VAS and the HIRS spectral bands, synthetic VAS and HIRS radiances for each of the 1200 soundings were computed. Then regression matrices were formed to relate the 12 VAS spectral radiances to the 19 HIRS spectral radiances for several different viewing angles. A VAS radiance for spectral band $\nu_i$ detected at viewing angle $\theta$, $R_V(\nu_i, \theta)$, can be estimated from HIRS radiances by the relation

$$R_V(\nu_i,\theta) = \sum_j R_H(\nu_j,0)\, a(\nu_j,\theta)$$

where $R_H(\nu_j, 0)$ is the HIRS radiance for spectral band $\nu_j$ detected at nadir and $a(\nu_j, \theta)$ is the regression coefficient of band $\nu_j$ for viewing angle $\theta$. Comparisons of VAS radiances and HIRS estimates of VAS radiances were made for several different days.

VAS dwell soundings from roughly 50°N to 20°N north latitude were accomplished in less than two hours on October 11 and December 9, 1980 and January 19, 1981 starting at 1245 GMT, 1532 GMT, and 1532 GMT respectively. NOAA-6 data over the United States for the same days were available at 1310 GMT, 1443 GMT, and 1404 GMT respectively. The VAS radiances for clear fields of view were

estimated from viewing angle corrected HIRS radiances close in time (within 90 minutes) and space (within 20 km). The fields of view were selected over uniform areas, such as cloudless water and plain regions. Figure I.2 shows the fields of views selected from October 11, 1980 data; cloudy regions were carefully avoided on this day and on the other days.

Table I.3 shows the comparison of VAS radiances and VAS radiance estimates from HIRS for the twelve VAS spectral bands (note: the brightness temperatures of the Planck radiances are recorded). The larger errors in some of the VAS bands have special explanations: bands 1 and 2 have been sampled with reduced spin budgets to save time therefore the signal to noise enhancement is not as good as it should be; window band 12 includes reflected solar contributions which cannot easily be corrected; and window bands 7, 8, and 12 are most sensitive to good navigation and time coincidence. The results for the window bands should be viewed cautiously.

The comparisons of October 11, 1980 are somewhat more credible since the NOAA-6 and VAS data acquisition occurred at nearly the same time; the other comparisons use data separated by 60 to 90 minutes but were made in regions where the weather was not changing rapidly. The VAS 15$\mu$ $CO_2$ bands 2, 3, and 4 show a consistent negative bias with respect to the HIRS predictions; the VAS $H_2O$ bands 7 and 9 show a positive bias.

The general agreement between the VAS and the HIRS is surprisingly good. The NOAA-6 brightness temperatures are only known to within 1°C so most of the comparisons are as good as can be expected.

The VAS radiances were also compared to the Limited Fine Mesh (LFM) analysis of radiosonde data over a period covering the last four months. Table I.4 shows the comparison. Data for the window bands is not presented because no reliable surface analysis was available. The relative errors are

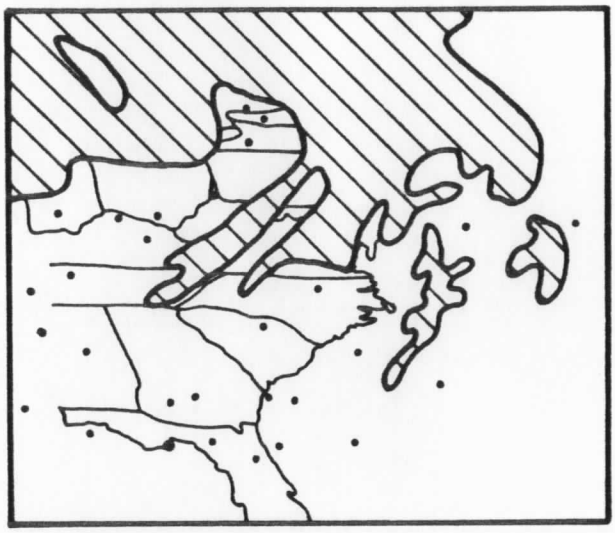

Figure I.2 Clear Fields of View Chosen for VAS Radiance Comparison with VAS Radiance Estimate from HIRS (Cloudy areas indicated) on October 11, 1980 between 1245 GMT and 1437 GMT.

Table I.3 VAS Radiances (brightness temperatures) Compared to VAS Radiance (brightness temperature) Estimates from HIRS Data

| VAS Bands | | HIRS Bands | | $B^{-1}(R_v^{est}) - B^{-1}(R_v)$ | | | | | |
|---|---|---|---|---|---|---|---|---|---|
| | | | | Oct. 11[b] | | Dec. 9[b] | | Jan. 19[b] | |
| # | $\nu(cm^{-1})$ | # | $\nu(cm^{-1})$ | abs(°C) | rel(°C) | abs(°C) | rel(°C) | abs(°C) | rel(°C) |
| 1 | 679 | 2 | 679 | .72 | 1.54 | .13 | 1.22 | .94 | 1.38 |
| 2 | 691 | 3 | 691 | 1.59 | 1.42 | 1.11 | .74 | .82 | 1.01 |
| 3 | 702 | 4 | 704 | 2.17 | .57 | 2.05 | .44 | 1.65 | .77 |
| 4 | 714 | 5 | 716 | 1.64 | .55 | .81 | .64 | 1.28 | .40 |
| 5 | 750 | 7 | 748 | 1.86 | .54 | -.49 | .72 | -1.03 | .45 |
| 6 | 2210 | 14 | 2212 | 1.30 | .52 | -.47 | .70 | -.33 | .60 |
| 7 | 790 | 10 | 1217[c] | -2.93 | 1.11 | -3.95 | .80 | -5.61 | .61 |
| 8 | 895 | 8 | 900 | .43 | 1.28 | -1.98 | .84 | -3.61 | .92 |
| 9 | 1377 | 11 | 1363 | -1.58 | 1.00 | -2.05 | .84 | -1.21 | 1.29 |
| 10 | 1487 | 12 | 1484 | -.09 | .99 | -.64 | 1.27 | .12 | .99 |
| 11 | 2250 | 15 | 2240 | 1.92 | .60 | .84 | .80 | .95 | 1.39 |
| 12 | 2535 | 18 | 2511 | -1.90 | 1.43 | 2.48 | 1.94 | -.52 | 1.84 |

a. The HIRS band closest to the VAS band is listed; all HIRS bands enter in the determination of $R_v^{est}$ through the regression relation.

b. The number of comparisons for the different days is 28, 21, and 22 respectively.

c. The transmittance of HIRS band 10 is similar to that of VAS band 7 although the frequencies are different.

Table I.4 VAS Radiances (brightness temperatures) Compared to Radiances (brightness temperatures) Determined from LFM Analysis of Radiosonde Data

| Band | $B^{-1}(R_{LFM}) - B^{-1}(R_V)^a$ | |
|---|---|---|
| | abs(°c) | vel(°c) |
| 1 | 1.3 | 4.6 |
| 2 | 3.2 | 3.1 |
| 3 | 2.8 | 1.6 |
| 4 | 1.7 | 1.4 |
| 5 | .3 | .8 |
| 6 | 1.1 | .7 |
| 7 | - | - |
| 8 | - | - |
| 9 | .8 | 3.1 |
| 10 | 1.9 | 1.4 |
| 11 | 2.1 | 2.5 |
| 12 | - | - |

[a] statistics are based on comparisons made over the past four months

around 1.5°C except for the noisy bands 1, 2, 9, and 11 and are within the expected accuracy of the comparison. However the VAS radiances (or brightness temperatures) for bands 2 through 4 are consistently lower than the corresponding values from the radiosonde analysis. This trend was also observed in the HIRS predictions (see the preceeding paragraphs) and in the prelaunch analysis of vacuum test data (see page 15 of the Prelaunch Study Report of VAS-D Performance). The VAS calibration algorithm is producing values that are roughly 2 to 3°C below the "true" values for bands 2 through 4.

Another evaluation of the inflight calibration was accomplished by comparing the temperature profile derived from VAS radiance data in the twelve spectral bands with a time and space coincident radiosonde derived temperature profiles. The VAS sounding retrieval method is the iterative inverse solution of the radiative transfer equation (see Applied Optics, 9, 1970, pp 1993-1999 for article by W. L. Smith, "Iterative Solution of the Radiative Transfer Equation for the Temperature and Absorbing gas Profile of an Atmosphere".) Currently, a forecast temperature and moisture field valid at 1200 GMT of each day is obtained from the National Meteorological Center which is used to obtain initial profiles for the iterative solution. The same forecast is used throughout the day to insure that diurnal variations resulting in the VAS retrievals are due solely to the diurnal variations in the atmospheric radiance to space observed by VAS. The bias errors listed in Table I.4 are removed from the radiances prior to the retrieval. Figure I.3 compares soundings near Rapid City, SD for approximately 9 AM and 3 PM local daylight time with radiosondes at 7 AM and 7 PM local daylight time. The variations indicated by the VAS soundings (a diurnal warming below 500 mb) are supported by the radiosonde observations. The profiles are typically within 1 or 2°C of one

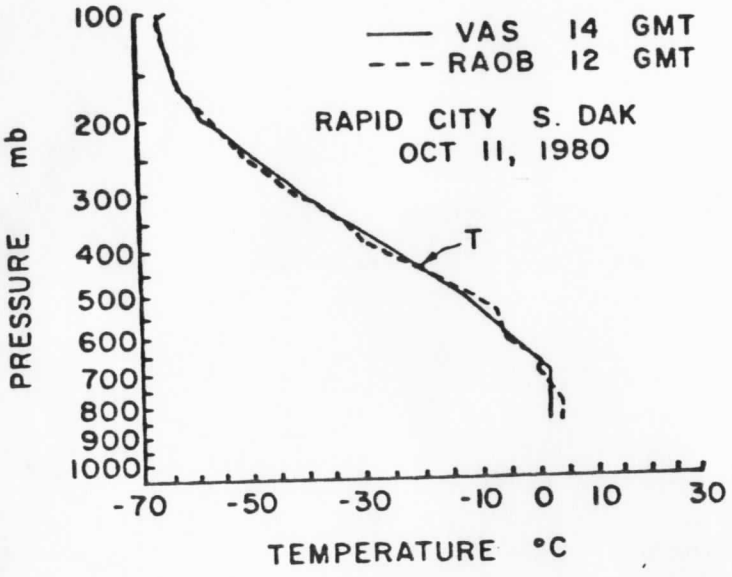


a.

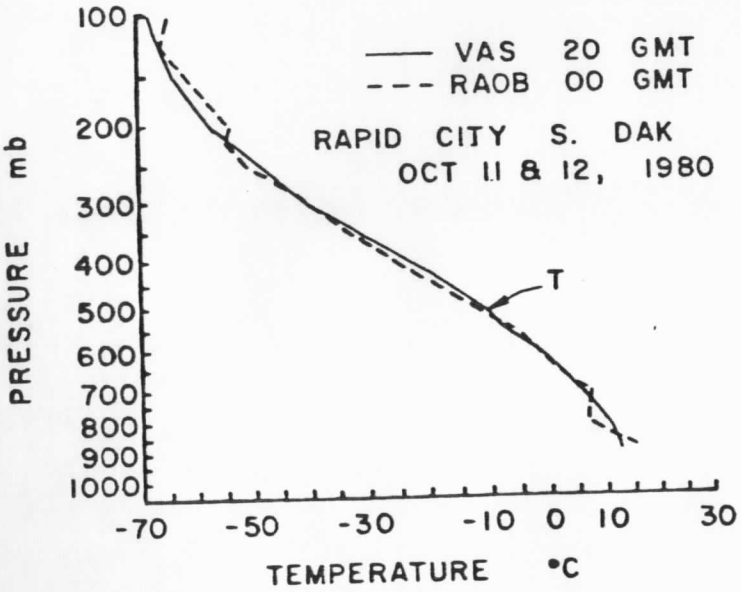


b.

Figure I.3 VAS Soundings Compared to Radiosondes

another; maximum deviations of 5°C are occasional. The agreement in temperature is as good as should be expected between these two different types of sounding observations.

Another similar comparison was accomplished on December 3, 1980 with radiosondes from Nashville, TN. The results are shown in Figure I.4. Again the diurnal warming in the lower atmosphere is observed by both the VAS and the radiosondes to an agreement of 1 or 2°C. VAS can clearly depict time variations in the atmospheric state.

Efforts to use the moon as a source of calibration for the VAS were made, however the results were not useful. The radiation from the moon either saturated the VAS IR detectors (the sunlight portion of the moon) or was not detected by the VAS IR detectors (the shaded portion of the moon). The dynamic range of the VAS detectors did not accomodate our moon calibration plans.

In summary, the VAS radiance have a negative offset for the upper atmospheric $CO_2$ bands (bands 2, 3, and 4) of 2 to 3°C. After removing this offset, the derived temperature profiles agree very well with radiosonde data. The VAS radiances are consistent with the HIRS data, considering the offsets mentioned above.

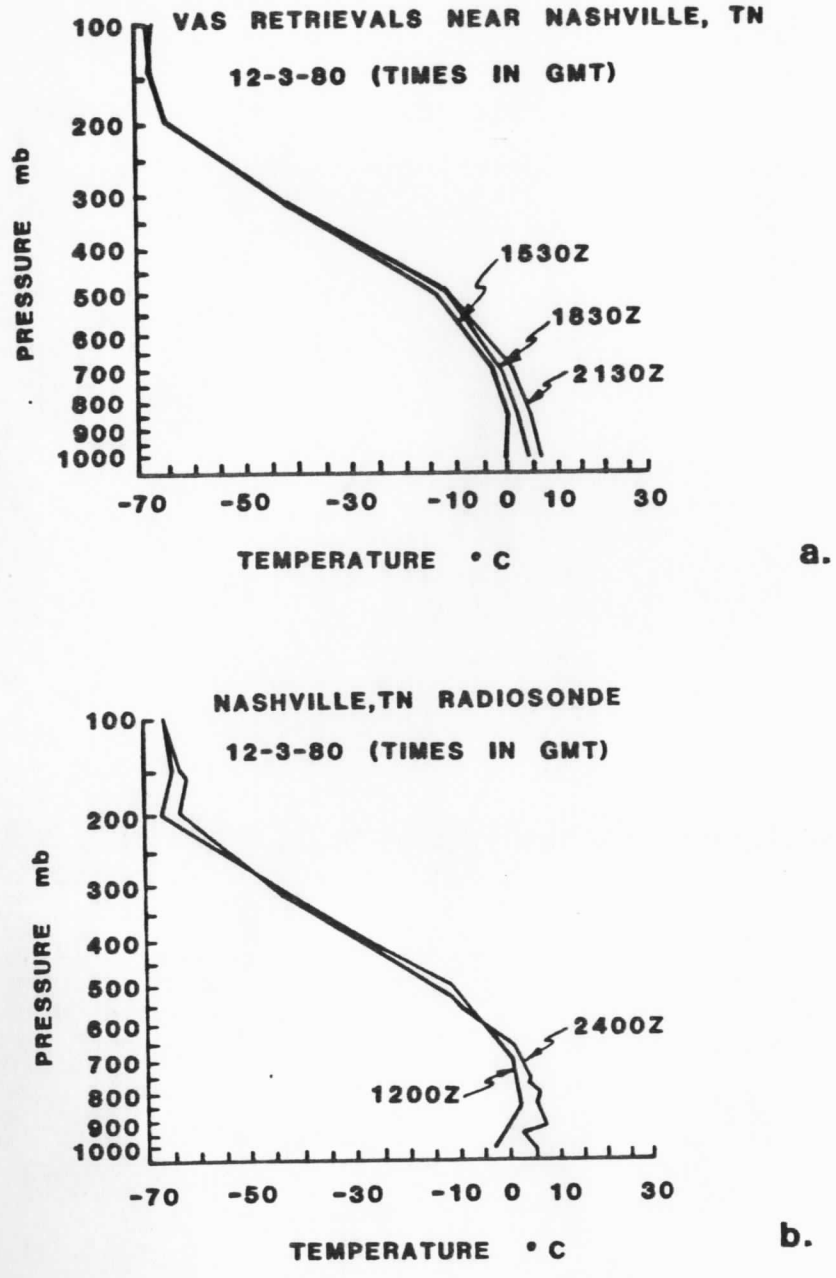


Figure I.4 VAS Soundings Compared to Radiosondes

## II. INFLIGHT VAS-D DETECTOR NOISE REDUCTION ANALYSIS

The VAS can determine special radiances over regions of interest to the required sounding accuracy of .25 ergs/(sec · $cm^2$ · $cm^{-1}$) only by averaging many individual measurements which have noise contributions that are significantly correlated to noise on preceding and following measurements. From inflight raw data, the effects of noise correlation were determined and the spin budget was updated.

In the October 11, 1980 dwell sounding data from 1245 GMT near 55°N, a sizeable space view allows us to calculate the autocovariance function and the spin budget for the large detectors. Figure II. 1 shows the autocovariance of noise as a function of sampling interval in the large detectors derived from inflight data and from prelaunch test data. The comparison is very good. The InSb noise is a little less correlated than expected, the large HgCdTe noise a little more. This close agreement is confirmed in the spin budget summary in Table II. 1. The updated inflight spin budget is 10% lower than the corrected prelaunch estimate. Band 2 values are suspect since it was under sampled to save time.

Continued monitoring of the VAS-D spin budget revealed seasonal variations; changes in the nominal scanner temperature, which varies with the time of the year, cause a 10% increase in detector responsivity in going from winter to summer. Prelaunch estimates were based on summer nominal scan temperatures, therefore spin budget calculations in winter should show a 20% increase. Table II. 2 corroborates this trend. As summer comes closer the spin budget should begin to decrease again.

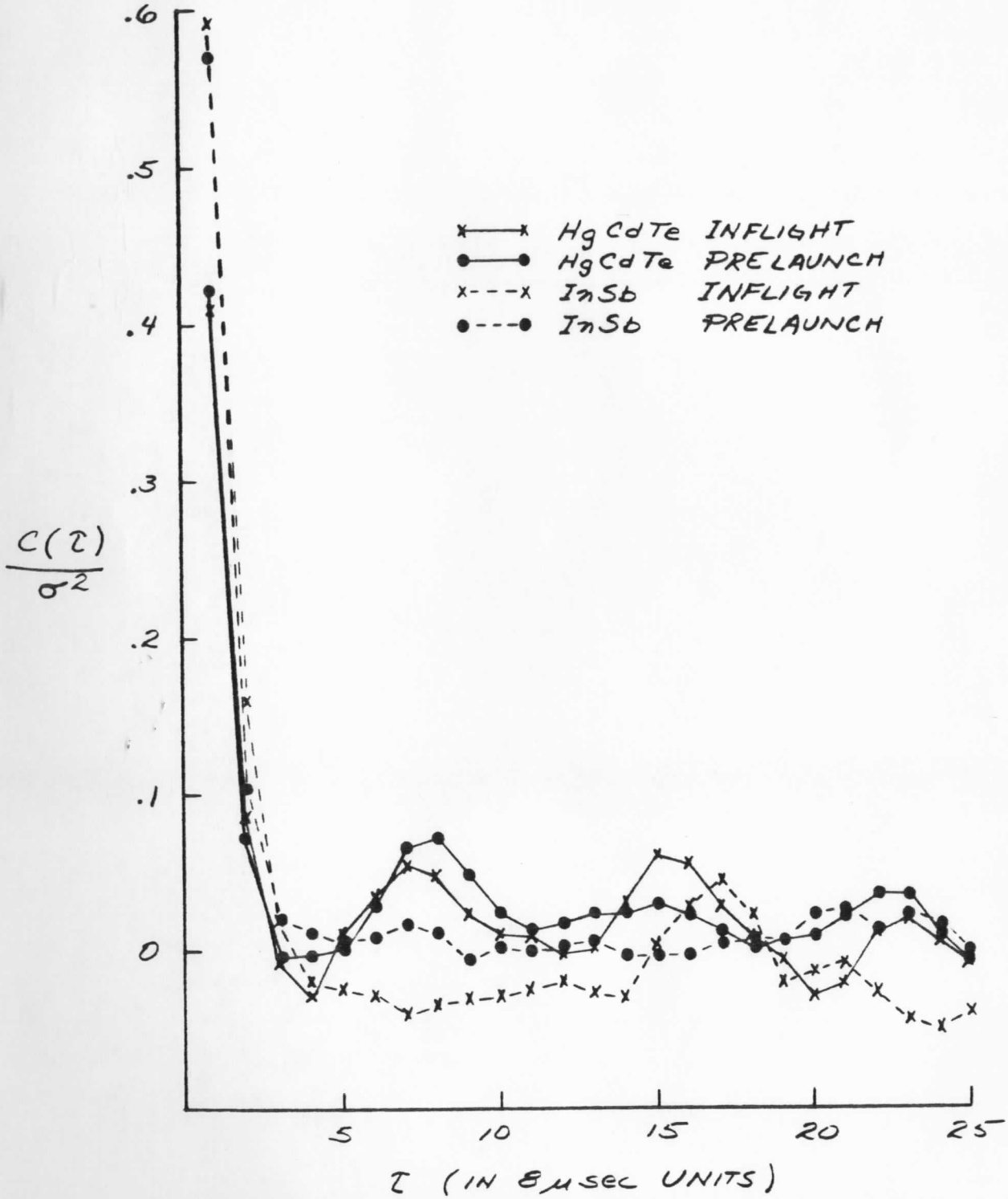


FIGURE II. 1 AUTOCOVARIANCE OF NOISE $C(\tau)/\sigma^2$ AS A FUNCTION OF SAMPLING INTERVAL $\tau$ IN LARGE DETECTORS EVALUATED FROM INFLIGHT DATA AND FROM PRELAUNCH TEST DATA.

Table II. 1 Inflight Spin Budget of VAS D Large Detectors

| Band | σ(erg/etc) | | Spin Budget | |
|---|---|---|---|---|
| | inflight | prelaunch | inflight | prelaunch |
| 1L | 4.13 | 4.93 | 1 | 2 |
| 2L | 2.53 | 3.26 | 14 | 24 |
| 3L | 1.76 | 1.79 | 9 | 9 |
| 4L | 1.49 | 1.77 | 7 | 8 |
| 5L | 1.13 | 1.33 | 4 | 5 |
| 6L | .028 | .028 | 10 | 9 |
| 7L | 1.07 | 1.00 | 3 | 3 |
| 8L | .12 | .14 | 1 | 1 |
| 9L | 1.23 | 1.38 | 12 | 11 |
| 10L | .31 | .33 | 2 | 2 |
| 11L | .026 | .027 | 8 | 8 |
| 12L | .007 | .008 | 1 | 1 |
| | | | 72 | 83 |

Table II.2 Time Variations of VAS-D Large Detector Spin Budget

| Band | σ(erg/etc) and Spin Budget | | | | | | | |
|---|---|---|---|---|---|---|---|---|
| | 10/11/80 | | 11/7/80 | | 12/4/80 | | 2/3/81 | |
| 1L | 4.13 | 1 | 4.31 | 1 | 4.84 | 2 | 5.24 | 2 |
| 2L | 2.53 | 14 | 2.91 | 19 | 3.00 | 21 | 3.22 | 23 |
| 3L | 1.76 | 9 | 1.98 | 10 | 1.97 | 10 | 1.85 | 9 |
| 4L | 1.49 | 7 | 1.80 | 8 | 1.85 | 8 | 1.86 | 8 |
| 5L | 1.13 | 4 | 1.27 | 5 | 1.34 | 5 | 1.35 | 5 |
| 6L | .028 | 10 | .035 | 13 | .032 | 12 | .036 | 13 |
| 7L | 1.07 | 3 | 1.01 | 3 | 1.02 | 3 | 1.07 | 3 |
| 8L | .12 | 1 | .21 | 1 | .25 | 1 | .18 | 1 |
| 9L | 1.23 | 12 | 1.42 | 14 | 1.48 | 14 | 1.48 | 14 |
| 10L | .31 | 2 | .32 | 2 | .37 | 2 | .45 | 3 |
| 11L | .026 | 8 | .030 | 10 | .030 | 11 | .033 | 11 |
| 12L | .007 | 1 | .008 | 1 | .008 | 1 | .008 | 1 |
| | | 72 | | 87 | | 90 | | 93 |

Total Spin Budget

# III. INFLIGHT DETERMINATION OF MISREGISTRATION OF VAS-D IMAGES

The retrieval techniques for obtaining clear column radiances from cloudy scenes rely on the multispectral viewing of the same scene within the instrument field of view. Preliminary determinations of the misregistration of images of the IR window channels (band 8 using HgCdTe detectors, band 12 using InSb detectors) and the visible channel were made from January, 1981 images of the moon. Because of the sharp delineation of the hot bright moon with cold dark space these images offer the best opportunity for accurate misregistration measurements. It was generally found that the IR image is east and south of the visible image. Table III.1 summarizes our findings. These misregistrations are corrected before any analysis of the sounding data can occur.

Table III.1 Misregistration of VAS-D Images

East West

| A \ B | Visible | HgCdTe(L) | HgCdTe(S) | InSb |
|---|---|---|---|---|
| Visible | — | .34 | .50 | .76 |
| HgCdTe(L) | -.34 | — | .16 | .42 |
| HgCdTe(S) | -.50 | -.16 | — | .26 |
| InSb | -.76 | -.42 | -.26 | — |

Image A is X milliradians west of Image B

North South

| A \ B | Visible | HgCdTe(L) | HgCdTe(S) | InSb |
|---|---|---|---|---|
| Visible | — | .17 | .17 | .17 |
| HgCdTe(L) | -.17 | — | .0 | .0 |
| HgCdTe(S) | -.17 | .0 | — | .0 |
| InSb | -.17 | .0 | .0 | — |

Image A is X milliradians north of Image B

# APPENDIX A. VAS-D GENERAL INFORMATION

## Detectors

The loss of the upper large HgCdTe detector leaves the VAS with five functioning detectors. Contiguous imaging or sounding with the large HgCdTe detectors requires that the modes of operation be adjusted.

## Dwell Sounding

Contiguous sounding with all twelve spectral bands can be accomplished only if sudmodes 1 and 3 are programmed for 2 steps (or less). In the 2-Dwell-2-Dwell scan pattern to achieve adequate signal to noise enhancement a full spin budget must be assigned to the spectral bands utilizing the large HgCdTe detector and half the spin budget can be assigned to those bands utilizing the large InSb detectors. Table A. 1 shows the October 11, 1980 inflight spin budget (see Section II) adjusted accordingly.

The contiguous sounding rate, instead of being 34.9 km/min in the 6-Dwell-2-Dwell mode, is 20.3 km/min in the 2-Dwell-2-Dwell mode which is 1.7 times as long.

## Multispectral Imaging

Contiguous multispectral images can be formed using either one set of small HgCdTe detectors and two sets of large InSb detectors, one set of small HgCdTe detectors and one set of large HgCdTe detectors, two sets of large InSb detectors and one set of large HgCdTe detectors, or two sets of large HgCdTe detectors. Images derived from the InSb detectors will be a composite of information from both detectors whereas the images derived from the large HgCdTe detector come from that detector alone.

The effect of the missing large HgCdTe is to limit the number of simultaneous images available in those bands that use the HgCdTe detectors.

Table A. 1 2-Dwell-2-Dwell Spin Budget

| Band | Detector | SB |
|---|---|---|
| 1 | H | 1 |
| 2 | H | 14 |
| 3 | H | 9 |
| 4 | H | 7 |
| 5 | H | 4 |
| 6 | I | 5[a] |
| 7 | H | 3 |
| 8 | H | 1 |
| 9 | H | 12 |
| 10 | H | 2 |
| 11 | I | 4[a] |
| 12 | I | 1[a] |

[a] One-half the nominal value; adequate signal to noise is achieved by averaging coverage of upper and lower InSb detectors.

## APPENDIX B. CORRECTED VAS-D PRELAUNCH ESTIMATES OF DETECTOR NOISE

Due to a misunderstanding with SBRC, the UW analysis of VAS-D large detector single sample noise included the effects of radiance losses in the calibration test equipment twice. The 12% calibrator reflectance losses were compensated for by SBRC and again by UW. This error has been corrected and Table B.1 should replace Table II.1 on page 28 of the Prelaunch Study Report of VAS-D Performance.

Table B.1 Corrected Prelaunch Estimate of VAS D Large Detector Spin Budget

| Band | $\sigma$(erg/etc) | I | $\sigma_M$(erg/etc) | $\sigma_{Req}$(erg/etc) | Spin Budget |
|---|---|---|---|---|---|
| 1U+ | 5.57 | 12.88* | .43 | .25 | 3 |
| 1L | 4.93 | 13.52* | .36 | .25 | 2 |
| 2U | 3.39 | 2.49 | 1.36 | .25 | 30 |
| 2L | 3.26 | 2.67 | 1.22 | .25 | 24 |
| 3U | 2.40 | 2.54 | .94 | .25 | 14 |
| 3L | 1.79 | 2.46 | .73 | .25 | 9 |
| 4U | 2.21 | 2.54 | .87 | .25 | 12 |
| 4L | 1.77 | 2.52 | .70 | .25 | 8 |
| 5U | 1.49 | 2.57 | .58 | .25 | 6 |
| 5L | 1.33 | 2.53 | .53 | .25 | 5 |
| 6U | .027 | 2.37 | .012 | .004 | 9 |
| 6L | .028 | 2.39 | .012 | .004 | 9 |
| 7U | 1.31 | 2.58 | .51 | .25 | 4 |
| 7L | 1.00 | 2.41 | .41 | .25 | 3 |
| 8U | .17 | 2.60 | .06 | .25 | 1 |
| 8L | .14 | 2.32 | .06 | .25 | 1 |
| 9U | 1.61 | 2.56 | .63 | .15 | 18 |
| 9L | 1.38 | 2.82 | .49 | .15 | 11 |
| 10U | .31 | 2.38 | .13 | .10 | 2 |
| 10L | .33 | 2.55 | .13 | .10 | 2 |
| 11U | .026 | 2.39 | .011 | .004 | 8 |
| 11L | .027 | 2.39 | .011 | .004 | 8 |
| 12U | .007 | 2.38 | .003 | .004 | 1 |
| 12L | .008 | 2.37 | .003 | .004 | 1 |
| Total U | | | | | 108 |
| L | | | | | 83 |

*Improvement factor for band 1 is evaluated for samples from 150 x 150 $km^2$: for all other bands it is evaluated for samples from 30 x 30 $km^2$.

+U indicates upper, L indicates lower.